

Novel Tools and Methods

Photothrombotic Middle Cerebral Artery Occlusion in Mice: A Novel Model of Ischemic Stroke

Emilia Conti,^{1,2,6,†} Noemi Carlini,^{1,2} Benedetta Piccardi,^{3,6,†} Anna Letizia Allegra Mascaro,^{1,2,6,*†} and Francesco Saverio Pavone^{2,4,5,*}

<https://doi.org/10.1523/ENEURO.0244-22.2022>

¹Neuroscience Institute, National Research Council, 56124 Pisa, Italy, ²European Laboratory for Non-Linear Spectroscopy, 50019 Sesto Fiorentino, Italy, ³Neurofarba Department, University of Florence, 50139 Florence, Italy, ⁴Department of Physics and Astronomy, University of Florence, 50019 Sesto Fiorentino, Italy, ⁵National Institute of Optics, National Research Council, 50019 Sesto Fiorentino, Italy, and ⁶Translational Research on Stroke (TREES) Working Group, Florence, Italy

Abstract

Stroke is one of the main causes of death and disability worldwide. Over the past decades, several animal models of focal cerebral ischemia have been developed allowing to investigate pathophysiological mechanisms underlying stroke progression. Despite intense preclinical research efforts, the need for noninvasive mouse models of vascular occlusion targeting the middle cerebral artery yet avoiding mechanical intervention is still pressing. Here, by applying the photothrombotic stroke model to the distal branch of the middle cerebral artery, we developed a novel strategy to induce a targeted occlusion of a large blood vessel in mice. This approach induces unilateral damage encompassing most of the dorsal cortex from the motor up to the visual regions 1 week after stroke. Pronounced limb dystonia one day after the damage is partially recovered after one week. Furthermore, we observe the insurgence of blood vessel leakage and edema formation in the peri-infarct area. Finally, this model elicits a notable inflammatory response revealed as a strong increase in astrocyte density and morphologic complexity in the perilesional region of the cortex compared with both other regions of the ipsilesional and contralesional hemispheres, and in sham-operated mice. To conclude, the stroke model we developed induces in mice the light-mediated occlusion of one of the main targets of human ischemic stroke, the middle cerebral artery, free from the limitations of commonly used preclinical models.

Key words: astrocytes; BBB permeability; clasping test; immunofluorescence; MCA photothrombotic occlusion

Significance Statement

Cerebral ischemic stroke is one of the leading causes of death and disability worldwide. Animal models represent a fundamental benchmark to investigate the pathophysiological mechanisms underlying the outcomes of stroke patients. Here, we developed and characterized a novel mouse model of stroke using the photothrombotic occlusion of the middle cerebral artery, one of the most common injury sites in stroke patients. The light-mediated occlusion leads in the acute phase to a severe motor deficit accompanied by the insurgence of blood–brain barrier extravasation, and the establishment of an inflammatory regime particularly pronounced in the peri-infarct cortex. This simple and highly reproducible model faithfully recapitulates human ischemic stroke avoiding common drawbacks of other stroke models.

Received May 31, 2022; accepted November 6, 2022; First published January 17, 2023.

The authors declare no competing financial interests.

Author contributions: A.L.A.M. designed research; E.C. and N.C. performed research; E.C. and N.C. analyzed data; E.C., A.L.A.M., and B.P. wrote the first draft of the manuscript.

Introduction

Stroke seriously threatens human health due to its high morbidity, disability, and mortality, thus representing a heavy financial and mental burden affecting families and society (Wafa et al., 2020). Intravenous thrombolysis and endovascular treatment are the standard therapies for patients with acute ischemic stroke. Unfortunately, due to the narrow time window of these treatments, possible treatment inefficacy in terms of recanalization, and the occurrence of reperfusion injury, there is still high variability in determining patient prognoses. These aspects draw the attention of preclinical research aiming to develop animal stroke models to further elucidate the pathophysiological mechanisms of injury and investigate the main processes of neurovascular disruption. In the past few decades, many strategies have been applied to induce ischemic insult in the brain tissue in animal models. Among the several models developed, middle cerebral artery (MCA) occlusion and photothrombosis (PT) are the most diffuse approaches, though they are characterized by some fundamental drawbacks (Macrae, 2011; Conti et al., 2021).

The intraluminal suture of the middle cerebral artery induces damage in the striatum and cortex, generating a sizable volume of penumbra (Carmichael, 2005) with the advantage of avoiding craniotomy and possible brain injury consequent to the surgery (Mies et al., 1991; Menzies et al., 1992). Nevertheless, MCA occlusion procedures are surgically demanding and may induce local traumatic effects (Kanemitsu et al., 2002). Moreover, in this model, the success rate of occlusion and the reproducibility of the infarct size are sometimes unsatisfactory (Yao et al., 2003; Macrae, 2011). On the other hand, the photothrombotic damage shares essential mechanisms occurring

with human stroke including the interruption of blood flow caused by platelet aggregation and alterations of the blood–brain barrier (BBB; Dietrich et al., 1987), guaranteeing a high reproducibility between subjects and the capability to easily target the lesioned area (Balbi et al., 2017; Allegra Mascaro et al., 2019). Nevertheless, this method, widely applied to induce small focal lesions, is poorly used in large blood vessels that would better represent severe human infarct. Having said that, a search for an occlusion model that encompasses the broad multiplicity of human ischemic progression is still a challenge for preclinical researchers.

Here, we developed and characterized in elderly mice a novel photothrombotic model of the MCA distal branch. We performed *in vivo* evaluations of mouse behavior and body weight 24 h and 7 d after stroke induction. Then, we quantified the extension of the lesion through *ex vivo* immunostaining. Finally, we characterized BBB permeability 24 h after stroke and alterations of astrocytes morphology through *ex vivo* immunohistochemistry 7 d after PT.

Materials and Methods

Mice

All procedures involving mice were performed in accordance with the regulations of the Italian Ministry of Health Authorization number 723/2019. Mice were housed in clear plastic cages under a 12 h light/dark cycle and were given *ad libitum* access to water and food. We used a transgenic mouse line, C57BL/6J-Tg(Thy1-EGFP)MJrs/J, from The Jackson Laboratory. Twenty-nine mice were identified by earmarks and were numbered accordingly. Animals were randomly divided into the following two groups: stroke mice (MCAPT $n = 15$; EB $n = 6$) and sham-operated mice (Sham MCAPT, $n = 4$; Sham EB, $n = 4$). To perform the brain water content evaluation and wire-hanging behavioral test, we used eight mice (Sham, $n = 4$; MCAPT, $n = 4$). Sham-operated mice were subjected to the same surgery and procedure with respect to MCAPT mice except for the Rose Bengal injection, replaced by the injection of the same volume of saline. Each group contained comparable numbers of male and female mice. The age of mice (age range, 16–18 months) was consistent between groups.

Photothrombotic occlusion of the distal branch of the middle cerebral artery

Mice were anesthetized with isoflurane (4% induction, 1.5% maintenance, in 1 L/min oxygen). Body temperature was maintained at 37°C with a heating pad (ThermoStar Temperature Controller, RWD). Mice were placed on a surgery pad, lying on one side. To ensure the stability of the animal, the mouse mouth was secured to the incisor bar and then blocked to the surgery pad. The mouse tail was then tightened to the surgery pad. The muscle over the squamosal bone was stretched with surgical tape to ensure more stability during the surgery. The mouse hairs between the eye and the ear were removed and then the skin was cleaned with betadine and ethanol. Then, local anesthetic lidocaine 2% (20 mg/ml) will be applied. The skin over the squamosal bone was cut, and the muscle

This research was funded by the Regione Toscana-Bando Ricerca Salute 2018; by Grant 20RSVP for the project “NIMBLE: Integrating Novel Neuroimaging Measurements and Circulating Biomarkers for the Prediction of Secondary Injury following Stroke: from Bench to Bedside”; by the Fondazione Cassa di Risparmio di Firenze, Grant SIME 2018/1179 id#24055 for the project “STROKELAB2BED. Ictus Ischemico Acuto: dal Laboratorio al Letto del Malato. Studio di biomarcatori ematici e di neuroimaging come predittori di edema cerebrale, estensione della lesione ischemica e dell’outcome funzionale”; by the European Research Council (ERC) under the European Union’s Horizon 2020 Research and Innovation Programme under Grant no. 692943 (BrainBIT); and by the Bank Foundation Fondazione Cassa di Risparmio di Firenze Grant “Human Brain Optical Mapping.” A.L.A.M., F.S.P. providing funding for the study.

*A.L.A.M. and F.S.P. contributed equally as last senior authors.

[†]Translational RESEARCH on Stroke (TREES) Working Group (in alphabetical order): Allegra Mascaro, AL, Baldereschi M, Conti E, Di Carlo AS, Fainardi E, Kennedy J, Lombardo I, Nencini P, Palumbo V, Piccardi B, Sarti C, Sodero A, Tudisco L.

Acknowledgments: We thank Lapo Turrini [National Institute of Optics, Consiglio Nazionale delle Ricerche (CNR), Rome, Italy], Claudia Alia (Neuroscience Institute, CNR), and Alessandro Sodero (Neurofarba Department, University of Florence, Florence, Italy) for valuable scientific feedback and discussions. We also thank Riccardo Ballerini from the mechanical workshop at LENS (European Laboratory for Non-Linear Spectroscopy, Florence, Italy) for the production of custom pieces.

Correspondence should be addressed to Emilia Conti at conti@lens.unifi.it.

<https://doi.org/10.1523/ENEURO.0244-22.2022>

Copyright © 2023 Conti et al.

This is an open-access article distributed under the terms of the Creative Commons Attribution 4.0 International license, which permits unrestricted use, distribution and reproduction in any medium provided that the original work is properly attributed.

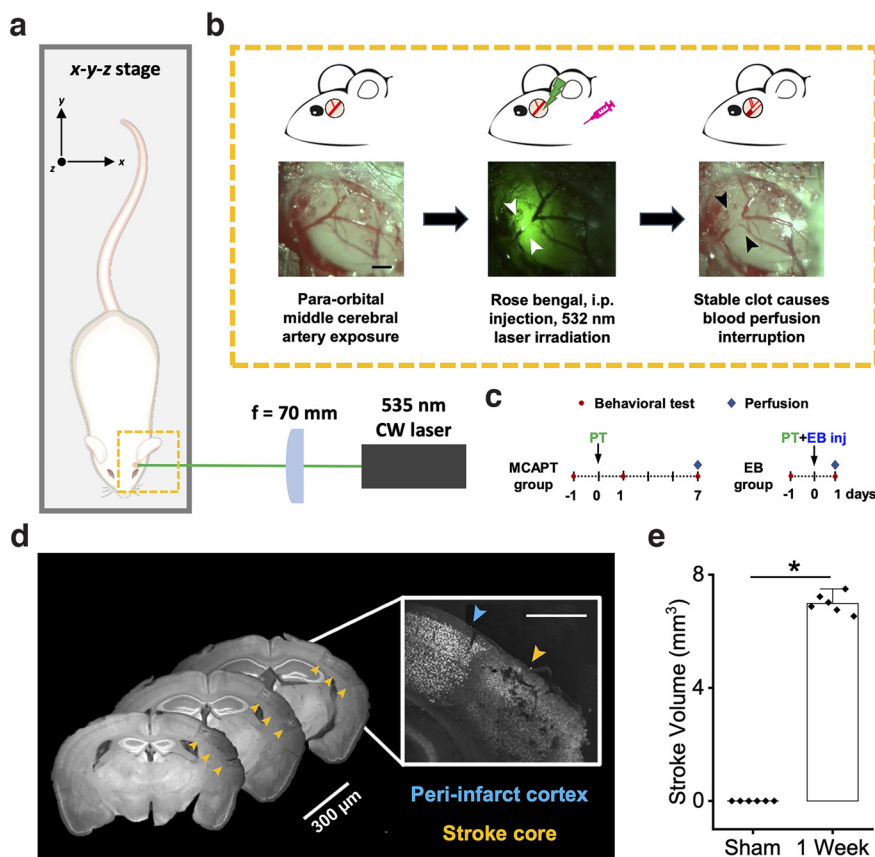


Figure 1. A novel single-vessel mouse model of photothrombotic stroke. **a**, Representative scheme of the custom-made setup for photothrombosis occlusion of the distal branch of the MCA; for details, see Materials and Methods. **b**, Representative scheme of the main steps of photothrombotic occlusion of the distal branch of the MCA and corresponding images acquired during surgery. Left, Exposure of the MCA after craniotomy. Middle, Highlighting of the laser irradiation focused on the blood vessel. Right, Formation of the clot. Scale bar, 0.5 mm. **c**, Experimental timeline for the two groups MCAPT and EB. **d**, Representative brain slices labeled with NeuN antibody. To quantify the lesion volume, we analyze one slice every 300 μm . The image in the inset, acquired with a confocal microscope, shows a boundary region between the periinfarct cortex and the stroke core. Scale bar, 1.25 mm. **e**, Right Quantification (mean \pm SEM) of stroke volume for the Sham group (0.1 ± 0.0001) and MCAPT group 1 week after photothrombosis ($6.9 \pm 0.1 \text{ mm}^3$). $*p = 2.29\text{E-}08$ based on one-way ANOVA followed by a *post hoc* Tukey's HSD test ($n = 6$). The error bar for the Sham group ($n = 4$) is below the minimum threshold. See also Extended Data Figure 1-1.

was detached from the skull and gently pushed down to expose the bone. We used a dental drill (Silfradent) to create a small craniotomy over the squamosal bone to expose the distal branch of the middle cerebral artery. Once removed the flap bone, a photosensitive dye, Rosebengal (0.2 ml, 10 mg/ml solution in Phosphate Buffer Saline (PBS), was intraperitoneally injected (Sigma Aldrich, USA). To induce PT, we developed a custom-made setup to finely controlled the laser irradiation on the distal branch of the middle cerebral artery (Fig. 1a). To this aim, we used a 532 nm laser (Laser Diode CPS532, ThorLabs) focused with a 70 mm lens onto the targeted blood vessel. The laser intensity at the focus was 128 mW/mm^2 (Watson et al., 2002). The mouse was held by the side on a stage, allowing displacements in the x-y-z directions (Translation Stage DTS25/M, Thorlabs).

Five minutes after the injection of the dye, a 532 nm green laser was focused before the MCA branch for 25 min to promote the formation of a stable clot and the consequent occlusion of the distal branch of the MCA. The green laser used for the experiments focused on the

blood vessel and did not heat the irradiated tissue near the MCA during photoirradiation, as shown by the presence of perfused blood vessels near the illumination site. At the end of the procedure, the muscle over the bone will be replaced and the skin sutured. Mice were placed in their cages until full recovery.

Ex vivo evaluation of blood–brain barrier permeability

To perform an *ex vivo* evaluation of blood–brain barrier permeability, we injected 0.20 ml of Evans Blue (EB) dye (0.20 mg/ml) into the mouse tail vein at the end of the surgery to occlude the distal branch of the MCA. Twenty-four hours after the injection, the animal was anesthetized by an intraperitoneal injection of ketamine (100 mg/kg) and xylazine (10 mg/kg) and then perfused with 100 ml of PBS to remove the blood from the brain tissue. The brain was then extracted and placed in paraformaldehyde (PFA) 4% for 1 h. Then the brain was sectioned with a brain matrix producing ~ 10 slices that were 1 mm thick.

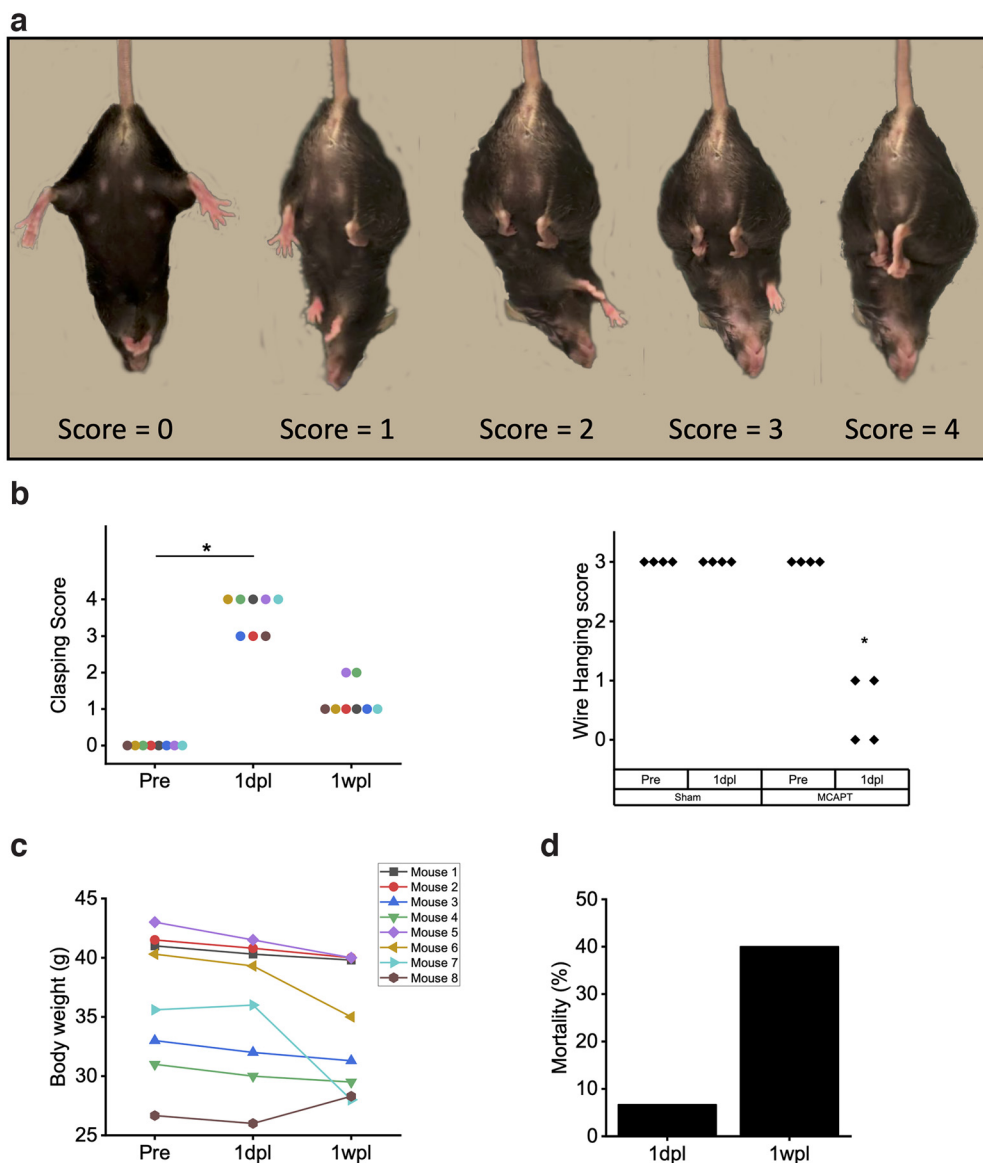


Figure 2. MCAPT induces severe dystonia in the acute phase after stroke: **a**, Representative pictures of mice during the clasping test. A score of 0 was assigned to mice with no clasping reflex; 1, 2, 3, and 4 were assigned respectively when one, two, three, and four limbs are retracted on the abdomen. **b**, Left, The clasping reflex revealed a tendency to higher clasping behavior after stroke both in the acute phase (at 1dpl) and at 1wpl. **p* value based on one-way repeated-measures ANOVA followed by a *post hoc* Tukey’s HSD test: Pre-1dpl, *p* = 0; Pre-1wpl, *p* = 1.57E-05; 1dpl-1wpl, *p* = 0. Right, The wire-hanging test revealed a decrease in the strength of mice forelimbs 24 h after the damage. **p* value based on one-way repeated-measures ANOVA followed by a *post hoc* Tukey’s HSD test: MCAPT Pre-1dpl, *p* = 1.83E-5; 1dpl Sham-MCAPT, *p* = 1.83E-5. **c**, The graph shows the weight of mice measured at the three time points. **d**, The graph shows the mortality rate 24 h and 1 week after the lesion (*n* = 15). See also Extended Data Figure 2-1.

Brain water content evaluation

The evaluation of brain water content was performed following the method previously applied by Kenne et al. (2012). Twenty-four hours after the occlusion of the MCA, mice were killed with an overdose of anesthetic. The brain was divided along the midline, and the contralateral and ipsilateral tissue was weighed right after removal to obtain wet weight (WW). The tissue was then dried at 60°C for 72 h and weighed to obtain dry weight (DW). Water content was calculated as follows: Water Content = (WW –

DW)/(DW). Tissue swelling was calculated as a percentage of the ratio between the variation of the wet weight and the initial wet weight: [(Final WW – Initial WW)/(Initial WW)] * 100.

Clasping test

The clasping behavior was induced by suspending the mouse from the base of the tail 10 cm above the cage for 20 s. We assigned a score of 0 for no clasp if the limbs are splayed outward away from the abdomen. If one limb is

retracted toward the stomach for >50% of the time suspended, we assigned a score of 1. If two limbs are retracted toward the stomach for >50% of the time suspended, we assigned a score of 2. If three limbs are retracted toward the stomach for >50% of the time suspended, we assigned a score of 3. If both forelimbs and hindlimbs touch and press on the stomach, indicating a severe clasp, we assigned a score of 4 (Fig. 2a). At the end of the test, the animal was placed into its cage.

Wire-hanging test

To evaluate grip strength, balance, and endurance 24 h after the injury, we tested mice in the wire-hanging test (Balkaya et al., 2013). Mice were brought by the tail near a 2-mm-thick metallic wire maintained 35 cm above a layer of bedding material to prevent injury to the animal in case of falls. When the animal hung to the wire with the forelimb, the mouse was released by the operator. If the animal reached one end of the wire the score was increased by 1. If the animal fell, the score was diminished by 1 and the elapsed time was noted. Mice performed three trials to obtain the final score.

Immunohistochemical analysis

For *ex vivo* investigation, stroke or sham-operated mice were transcardially perfused with 4% PFA on day 7 after surgery. Brains were cut using a vibrating-blade vibratome (Leica) to obtain 100- μ m-thick coronal sections that were used for immunostaining of the neuronal marker NeuN (1:1000; anti-NeuN chicken, Millipore) and glial fibrillary acidic protein (GFAP; 1:1000; anti-GFAP rabbit, Abcam).

The NeuN immunostaining was performed to quantify the lesion volume 1 week after PT. The stroke volume for each animal was calculated by summing up all damaged areas and multiplying the number by section thicknesses and by the spacing factor 4 (Conti et al., 2022). Images were acquired with a (Stemi 508, Carl Zeiss). The total volume in cubic millimeters is given as the mean \pm SE of all analyzed animals ($n=6$). The experimenter was blind to the experimental group of the samples.

The number of GFAP-positive neurons was analyzed using a confocal fluorescence microscope (model Eclipse TE 300, Nikon) with a Nikon Plan EPO 60 \times objective (numerical aperture 1.4, oil-immersion, Nikon). We decided to focus our investigation on the following four regions of interest (ROIs): the peri-infarct area [ischemic border zone ipsilesional (IBZ_{IL})]; a region in the ipsilesional hemisphere distant to the stroke core [remote zone IL (RZ_{IL})]; a region contralateral (CL) to the peri-infarct area [ischemic border zone CL (IBZ_{CL})]; and a region in the healthy hemisphere CL to the ischemic core (IC_{CL}). For each ROI (IBZ_{IL}, RZ_{IL}, IBZ_{CL}, IC_{CL}), we acquired three fields of view. The density of GFAP-positive cells was evaluated considering the following criteria: (1) the same brightness/contrast value was set for all images; (2) cells placed at the border of the image were not counted; (3) cells that were not clearly visible were excluded and therefore not counted; and (4) specific signals of the background were excluded.

The morphologic analysis of astrocytes was performed using two strategies: Sholl's method and the Skeleton analysis. For each of the five animals, three slices of the brain, central to the damage, were analyzed. In each slice, we acquired three images (212.13 \times 212.13 μ m) for each ROI, and in each image, we identified three astrocytes. One hundred eight astrocytes per animal were analyzed. We used four animals for the analysis of the sham mice. For each animal, we analyzed three slices, and for each slice we analyzed three astrocytes for each of the four ROIs (IBZ_{IL}, RZ_{IL}, IBZ_{CL}, IC_{CL}). A total of 144 astrocytes was analyzed.

By applying Sholl's method (ImageJ software), we isolated each individual astrocyte, and, starting from the soma, we drew concentric circles around it, at a distance of 3 μ m from each other. This method allows quantifying the number of intersections of each astrocytic process with a single circumference and the total number of intersections.

We used Skeleton analysis (ImageJ software) to determine the number and length of primary processes, the number of junctions, the number of end points, the average length of the processes, and finally the maximum length of the branches of the astrocytes. Since in Sham mice we did not reveal any significant differences among the four ROIs, we considered a mean value for each parameter in the main figures of the manuscript and added the Sham analysis for each ROI (IBZ_{IL}, RZ_{IL}, IBZ_{CL}, IC_{CL}) in the Extended Data Figs. 4-2, 5-1, 5-2.

Statistical analysis

All the analyses performed in both the *in vivo* and *ex vivo* experiments were performed blind. Moreover, all the data were independently evaluated by the two researchers that performed the experiments and the analysis. Results were considered statistically significant if their corresponding p value was ≤ 0.05 . OriginPro software (OriginLab) was used for all other statistical analyses. For all ANOVAs that were statistically significant, multiple comparisons among time points and different regions of the cortex were assessed using repeated-measures ANOVA followed by a *post hoc* Tukey's HSD test.

Results

A novel single-vessel photothrombotic stroke mouse model

We developed a novel method to permanently induce light-mediated occlusion of the distal branch of the MCA in mice (Fig. 1a,b). The MCA was exposed through a small craniotomy (Fig. 1b, left). Then, 5 min after the intraperitoneal injection of Rose Bengal, the MCA was illuminated for 25 min with a green laser (Fig. 1b, middle), which promoted the formation of a stable clot (Fig. 1b, right) and, consequently, blood perfusion interruption in the downstream brain tissue. We performed the MCAPT in two different experimental groups (Fig. 1c). In the first group (MCAPT) we performed behavioral experiments the day before the stroke (Pre) and then 24 hours (one day post lesion, 1dpl) and one week (one week post lesion, 1wpl) after the photothrombosis. After behavioral evaluations,

mice were perfused to perform *ex vivo* experiments. In the second group (EB), mice were tested 1 d before and 1 d after stroke. At the end of photothrombosis, we injected Evans Blue serum albumin-binding dye into the mouse tail vein to determine the presence of extravasation (i.e., hemorrhage and edema) in brain tissue 1 d after damage. For both experimental groups (MCAPT and EB), we performed a set of experiment in which mice were subjected to the same surgery and procedure with respect to MCAPT and EB mice, respectively, except for the Rose Bengal injection, which was replaced by injection of the same volume of saline. At the end of the experimental period, mice were killed to performed *ex vivo* evaluations (Extended Data Fig. 1-1). To quantify the lesion volume induced by the photothrombotic occlusion of the MCA 1 week after stroke, the perfused brain was cut into 100 μm coronal sections. The NeuN immunostaining highlighted a region of dead tissue affecting only the mouse cortex extending from motor regions up to visual areas, in the rostrocaudal direction (Fig. 1*d*), with an overall lesion volume of $6.9 \pm 0.1 \text{ mm}^3$ in stroked mice (Fig. 1*e*). Sham mice did not show any sign of tissue suffering ascribable to craniotomy or laser irradiation (Extended Data Fig. 1-1, panels 1–4).

MCAPT induces severe dystonia in poststroke acute phase

To assess the functional impairment caused by photothrombosis, we performed the clasping test (Guyenet et al., 2010; Miedel et al., 2017) at different time points (Fig. 2*a*). While in healthy conditions, all the mice splay the limbs outward, indicating the physiological reflex to grab something when hanged, 1 d after MCA photothrombosis we observed a considerable worsening of motor performance, only partially recovered 1 week after stroke (Fig. 2*b*). Then to better characterize motor performances in the acute phase after stroke, we tested a subgroup of mice in the wire-hanging test (MCAPT, $n = 4$; Sham, $n = 4$). While the final score remained unaltered 24 h after the surgery in Sham mice, we observed in MCAPT animals a severe worsening of the grip strength, balance, and endurance (Fig. 2*b*, right). Body weight evaluation did not highlight any significant difference before and after photothrombosis (Fig. 2*c*), though mouse body weight variations are higher in the MCAPT group compared with the Sham group (Extended Data Fig. 2-1*a*). The permanent occlusion of the distal branch of the MCA is lethal for 6.6% ($n = 1$) of mice 1 d after irradiation, and 40% ($n = 5$) 1 week after stroke (Fig. 2*d*).

MCAPT induces blood–brain barrier leakage and edema formation in the ipsilesional hemisphere

We then wondered whether the high percentage of mortality observed during the first week after the MCA occlusion (Fig. 2*d*) was caused by the emergence of blood–brain barrier alterations (i.e., hemorrhage and edema). To clarify this aspect, we used Evans Blue, an organic dye characterized by a very high affinity for serum albumin, which allows a rapid and low-cost assessment of BBB permeability (Saunders et al., 2015). The loss of blood–

brain barrier integrity and the consequent extravasation were evaluated by quantifying the presence of blue staining of cerebral tissue, caused by leakage of the dye from the blood vessels to the brain parenchyma (Stoll et al., 2009; Yang et al., 2017). Therefore, in EB mice ($n = 6$), we injected the Evans Blue dye into the mouse tail vein right after photothrombosis. Mice were then killed 24 h after the injection. While in Sham mice ($n = 4$) no evidence of blood–brain barrier alterations were revealed (Extended Data Fig. 1-1, panels 5–8), in MCAPT mice we observed that the diffusion of the dye affects a large portion of the ipsilesional hemisphere, extending both in the rostral direction up to the olfactory bulbs and in the caudal regions, (Fig. 3*a,b*). Moreover, the tissue appears to be swollen around the stroke core (Fig. 3*a*, black arrows). These animals, evaluated through the clasping test before (Pre) and 1 day after stroke (1dpl), showed behavioral deficits comparable to the MCAPT group and no consistent alterations in body weight (Extended Data Fig. 2-1*b,c*). In particular, mice with more severe impairment are characterized by a higher extension of extravasation (Fig. 3*c*). Since this preliminary evaluation suggested the presence of a barrier leak, to better quantify the presence of edema 24 h after the photothrombotic damage, we evaluated the brain water content of ipsilesional and contralesional hemispheres as a measure of cerebral edema (Kenne et al., 2012) in another group of mice (Sham, $n = 4$; MCAPT, $n = 4$). The comparison of the variation of water content between hemispheres of Sham with respect to MCAPT mice showed a significant increase in water after the photothrombotic occlusion of the MCA (Fig. 3*d*). Moreover, a significant increment of tissue swelling was observed in the MCAPT group, which was not found in Sham mice (Fig. 3*e*).

MCAPT increases astrocytes density and complexity in the peri-infarct cortex

To quantify the inflammation induced by the damage, we analyzed astrocytes in different regions of the brain in MCAPT and Sham mice. We identified the following four regions of interest (Fig. 4*a*) within the cortex: ipsilesional ischemic border zone (IBZ_{IL}), remote zone (RZ_{IL}), contralesional ischemic border zone (IBZ_{CL}), contralesional ischemic core (IC_{CL}), Extended Data Fig. 4-1. In the ischemic core (IC), no fluorescence signal was revealed. At a glance, as shown in Figure 4*b*, the IBZ_{IL} in MCAPT animals was characterized by an intense fluorescence signal compared with other regions. The analysis revealed an increase of GFAP-positive astrocytes in the peri-infarct area (IBZ_{IL}) of MCAPT animals with respect to Sham mice (Extended Data Fig. 4-2). Moreover, astrocyte density in the IBZ_{IL} of MCAPT mice was significantly higher with respect to other regions both in the ipsilesional and contralesional cortices (Fig. 4*c*, Extended Data Table 4-1). Then, by quantifying the number of branch intersections through Sholl analysis (Fig. 5*a*), we observed a significant increment of the intersection number (21–27 μm from the cell body) of IBZ_{IL} astrocytes compared with other regions of MCAPT mice (Extended Data Table 5-1). Conversely, in Sham animals, no differences were revealed between the ROIs at increasing distances from the cell body (Extended Data Fig. 5-1,

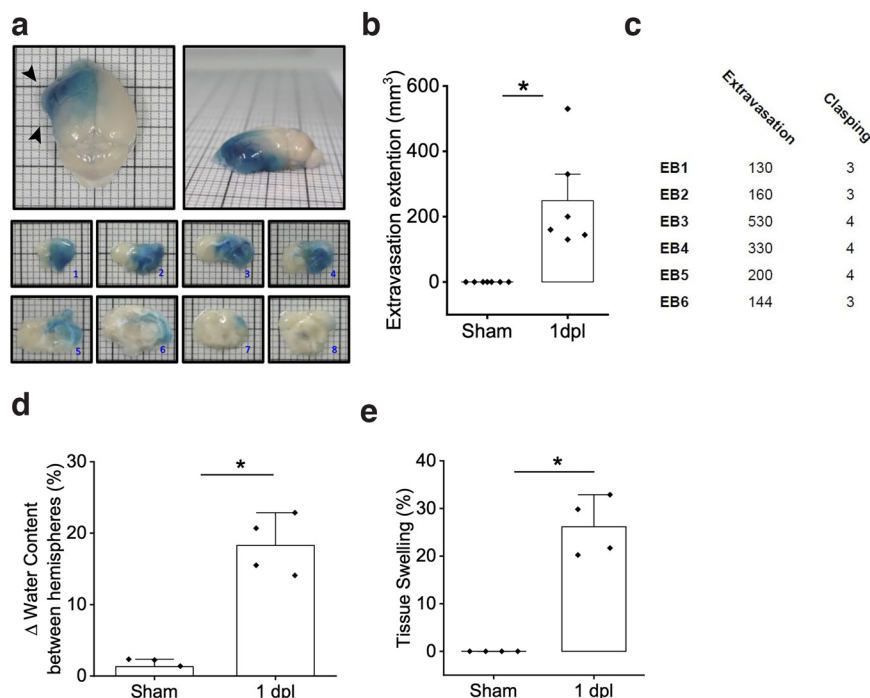


Figure 3. MCAPT induces blood–brain barrier leakage and edema formation in the ipsilesional hemisphere. **a**, Dorsal (left) and lateral (right) pictures of a representative MCAPT brain of a mouse injected in the tail vein with Evans Blue dye right after photothrombosis. **1–8**, Coronal sections of the same animal. Black arrows point to tissue swelling. **b**, *Ex vivo* quantification of the brain tissue presenting a blue signal in the Sham group and the EB group (1dpl) 1 d after the photothrombotic occlusion. * $p = 0.003$ based on one-way ANOVA followed by a *post hoc* Tukey’s HSD test ($n = 6$). **c**, The table shows the clasping test score and the extension of extravasation for each EB mouse. **d**, Brain water content evaluation 24 h after damage highlights the increase of wet weight in the ipsilesional hemisphere of MCAPT mice with respect to Sham mice. * $p = 0.003$ based on one-way ANOVA followed by a *post hoc* Tukey’s HSD test ($n = 4$). **e**, Tissue swelling evaluation 24 h after stroke shows the emergence of brain tissue distortion affecting the ipsilesional hemisphere of MCAPT mice. * $p = 0.0001$ based on one-way ANOVA followed by a *post hoc* Tukey’s HSD test ($n = 4$).

Extended Data Table 5-2, Table 5-3). Finally, to further investigate astrocyte morphology, we performed Skeleton analysis to quantify the length of astrocytic processes as well as the number of branches, junctions, and end points (Fig. 5c, Extended Data Fig. 5-2). Astrocyte morphology is consistent among all the ROIs in Sham mice (Extended Data Fig. 5-2b). In detail, astrocytes show a lower number of branches, junctions, and end points in all the analyzed regions compared with MCAPT mice (Fig. 5c, Extended Data Fig. 5-2b, Extended Data Tables 5-4, 5-5). Conversely, MCAPT mice showed strong differences in morphologic features between the regions observed (Fig. 5c, Extended Data Table 5-6). In particular, in the ipsilesional hemisphere the analysis revealed a significant difference in the number of branches, junctions, and end points between IBZ_{IL} and RZ_{IL}. Finally, in the contralesional hemisphere, all morphologic parameters were comparable between the two regions analyzed.

This aspect highlights the establishment of an inflammatory regime in the acute phase after stroke involving both hemispheres, though especially prominent in the periinfarct cortex of MCAPT mice.

Discussion

In this study, we adopted the photothrombotic technique to induce an ischemic occlusion of the distal branch of the middle cerebral artery in mice. Although a similar

approach was successful in rats (Watson et al., 1987) and rabbits (Zhao et al., 2002), and in a “tandem occlusion” through the ligation of the common carotid artery in mice (Sugimori et al., 2004), to the best of our knowledge, this is the first study showing its application in mice.

The occlusion of the MCA can be achieved with other strategies such as the intraluminal insertion of a filament, the endothelin-1 model, and the ligation or cauterization of the blood vessel, resulting in different postinjury complications (Gonzalez and Kolb, 2003). As previously discussed, the intraluminal suture of the MCA technique is a widely used animal model of stroke. However, the insertion of the filament leads to obstruction of the hypothalamic artery, thus inducing hyperthermia and a consequent increase of infarct volume, worsening functional outcome (Zhao et al., 1994; Reglodi et al., 2000). Moreover, this model shows high variability of the infarct size resulting in low reproducibility and an unsatisfactory success rate of occlusion (Howells et al., 2010). Furthermore, the surgery to access and manipulate the vasculature requires skilled and experienced hands (Howells et al., 2010). The endothelin-1 technique is another stroke model commonly used both in rats and mice, based on the local application of a vasoconstrictor agent. The procedure is easy to perform and allows the control of vessel vasoconstriction modulating the dose of the vasoconstrictive agent. However, this

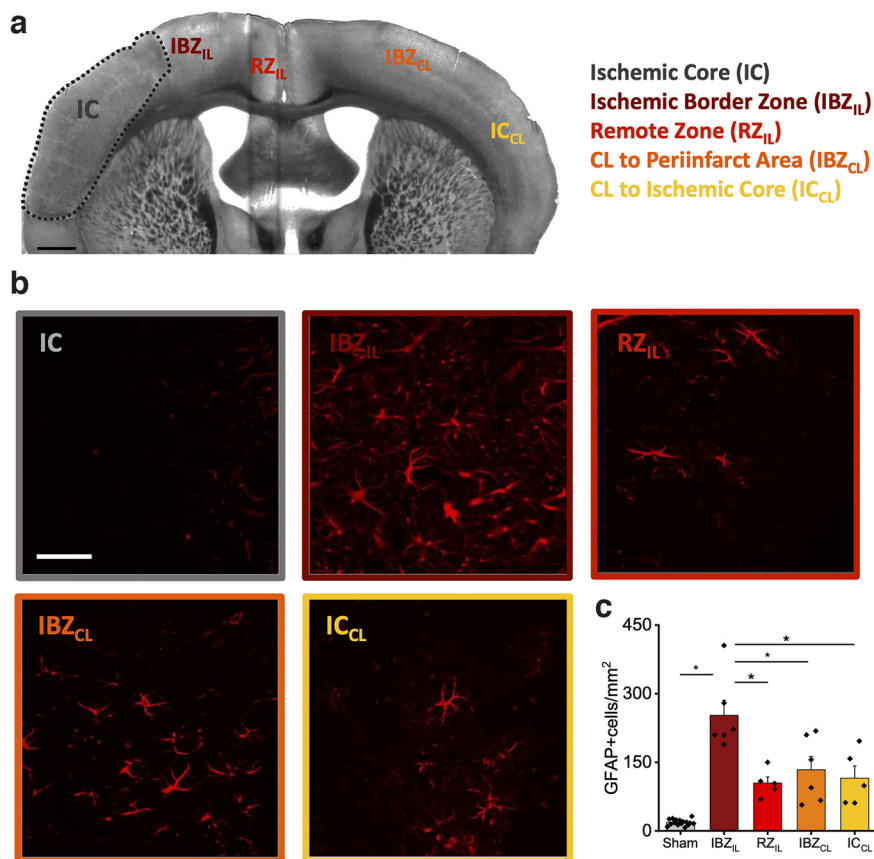


Figure 4. MCAPT increases astrocyte density in the peri-infarct area. **a**, A representative brain slice highlighted the IC and the 4 ROIs identified for the astrocytes analysis. Scale bar, 0.5 mm. **b**, Representative field of view of each ROI acquired with a confocal microscope. Scale bar, 45 μ m. **c**, The graph shows the density (average \pm SEM) of GFAP-positive cells in the 4 ROIs (IBZ_{IL} = 252.57 \pm 33.07; RZ_{IL} = 104.63 \pm 13.23; IBZ_{CL} = 133.64 \pm 29.11; IC_{CL} = 115.18 \pm 26.894). *p* value based on one-way ANOVA followed by a *post hoc* Tukey's HSD test. See Extended Data Table 4-1: IBZ_{IL}-RZ_{IL}, *p* = 0.00,721; IBZ_{IL}-IBZ_{CL}, *p* = 0.02,508; IBZ_{IL}-IC_{CL}, *p* = 0.01278. See also Extended Data Figures 4-1 and 4-2.

approach is characterized by high variability in stroke volume (Braeuninger and Kleinschnitz, 2009). Similarly, the cauterization of the MCA is characterized by low reproducibility (Mora-Lee et al., 2011) and presents several drawbacks, including possible damage to the dura mater and tissue surrounding the vessel. Furthermore, cauterization induces permanent damage, not amenable to reperfusion by removing the suture filament, or by light-induced recanalization thrombolytic agents (Ishrat et al., 2009). Conversely, the photothrombotic model has the advantage of inducing the formation of platelet-rich and fibrin-rich thrombi in the blood vessels of the irradiated site (Matsuno et al., 1993; Saniabadi et al., 1995). This approach is minimally invasive and is capable of inducing highly reproducible cortical damage both in rats and mice, targeting with high precision the location of ischemia (Macrae, 2011). Moreover, photothrombosis has the great advantage of tuning the plasma concentration of the dye, and the intensity and duration of the light to control the size and the depth of the lesion. Depending on the procedure applied, the target of photothrombosis ranges from an extended region of the cortex to a single capillary.

In previous studies, the photothrombotic approach was applied to single blood vessels within the mouse brain cortex (Shih et al., 2013). This strategy has on the one hand the advantage of being able to target the region of the damage to investigate the microscopic basis of cerebral ischemia, selecting a specific class of blood vessel (i.e., capillary or surface arteriole or venule) in a specific cortical area. By combining the stroke model with imaging setups equipped with multiple light sources, alterations of the vasculature (Clark et al., 2019; Sunil et al., 2020), and brain dynamics, such as cortical depolarizing waves, (Balbi et al., 2017) were monitored *in vivo*.

Here, by characterizing the photothrombotic occlusion of the distal branch of the MCA in mice, we observed the formation of a stable clot in the blood vessel after 25 min of laser irradiation that leads to reproducible extended damage in the mouse cortex 1 week after the lesion. Compared with both single-capillary and cortex-targeted photothrombosis, our model, targeting the distal branch of the MCA, induces a more severe lesion within the mouse brain cortex. Moreover, with respect to the cortical irradiation model, in which the distribution of pial microvasculature can vary between animals of different

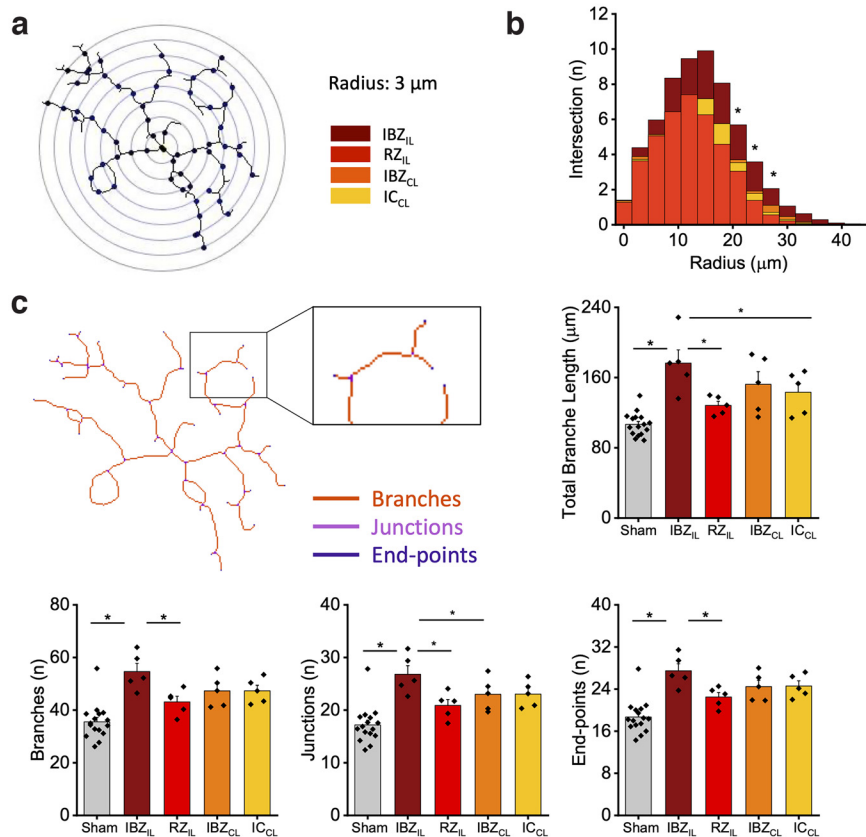


Figure 5. MCAPT increases astrocyte complexity in the peri-infarct area of MCAPT mice. **a**, Representative image of an astrocyte analyzed with the Sholl method. **b**, The graph shows the distribution of the number of intersections for each radius in the 4 ROIs. *p* value based on two-way repeated-measures ANOVA followed by a *post hoc* Tukey's HSD test. See Extended Data Tables 5-1, 5-2, and 5-3: radius 7: IBZ_{IL}-RZ_{IL}, *p* = 2.51E-08; IBZ_{IL}-IBZ_{CL}, *p* = 0.006; IBZ_{IL}-IC_{CL}, *p* = 0.006; radius 8: IBZ_{IL}-RZ_{IL}, *p* = 8.65E-07; IBZ_{IL}-IBZ_{CL}, *p* = 0.013; IBZ_{IL}-IC_{CL}, *p* = 1.72E-04; radius 9: IBZ_{IL}-RZ_{IL}, *p* = 6.82E-06; IBZ_{IL}-IBZ_{CL}, *p* = 0.029; IBZ_{IL}-IC_{CL}, *p* = 4.10E-04. **c**, Representative image of the same astrocyte in **a** analyzed with the Skeleton analysis. All the features of astrocytes in the 4 ROIs are shown as the average ± SEM. The intergroup statistical analysis was performed through a two-way repeated-measures ANOVA followed by a *post hoc* Tukey's HSD test; see Extended Data Table 5-4. The intragroup statistical analysis was performed through a one-way repeated-measures ANOVA followed by a *post hoc* Tukey's HSD test; see Extended Data Tables 5-5 and 5-6. Total branches length sham = 106.71 ± 3.32; IBZ_{IL} = 176.53 ± 15.04; RZ_{IL} = 128.32 ± 4.74; IBZ_{CL} = 152.23 ± 14.49; IC_{CL} = 143.28 ± 11.04; intergroup analysis: IBZ_{IL} MCAPT-Sham, *p* = 0.002; intragroup analysis: IBZ_{IL}-RZ_{IL}, *p* = 0.003; IBZ_{IL}-IC_{CL}, *p* = 0.033. Number of astrocytes, branches: Sham = 35.54 ± 1.68; IBZ_{IL} = 54.645 ± 3.126; RZ_{IL} = 43.127 ± 2.161; IBZ_{CL} = 47.307 ± 2.742; IC_{CL} = 47.341 ± 2.113; intergroup analysis: IBZ_{IL} MCAPT-Sham, *p* = 0.001; intragroup analysis: IBZ_{IL}-RZ_{IL}, *p* = 0.044. Number of astrocytes, junctions: Sham = 17.18 ± 0.87; IBZ_{IL} = 26.81 ± 1.63; RZ_{IL} = 20.89 ± 1.13; IBZ_{CL} = 23.01 ± 1.421; IC_{CL} = 23.04 ± 1.12; intergroup analysis: IBZ_{IL} MCAPT-Sham, *p* = 0.03; intragroup analysis: IBZ_{IL}-RZ_{IL}, *p* = 0.026; IBZ_{IL}-IC_{CL}, *p* = 0.042. Number of astrocytes, end points: Sham = 18.68 ± 0.77; IBZ_{IL} = 27.47 ± 1.34; RZ_{IL} = 22.49 ± 0.86; IBZ_{CL} = 24.47 ± 1.20; IC_{CL} = 24.58 ± 0.97; intergroup analysis: IBZ_{IL} MCAPT-Sham, *p* = 0.02; intragroup analysis: IBZ_{IL}-RZ_{IL}, *p* = 0.044. See also Extended Data Figures 5-1 and 5-2.

ages or strains (Labat-gest and Tomasi, 2013), the photothrombotic occlusion of the distal branch of the MCA enables high reproducibility. Furthermore, the model induces a strong behavioral deficit revealed by the clasping and wire-hanging tests, mimicking a severe human infarction. Moreover, the MCAPT induces a pronounced leakage of the BBB and edema formation, making it a suitable model to investigate the main consequences affecting human stroke patients (i.e., hemorrhagic transformation and cerebral edema). Indeed, during the acute phase postinjury, the strong behavioral impairment is accompanied by the alteration of the BBB. Previous studies using MCA occlusion to induce a cerebral stroke

observed an increase in BBB permeability in the acute phase after the damage (Belayev et al., 1996; Rosenberg et al., 1998; Candelario-Jalil et al., 2022). In particular, Fernandez-Lopez et al. (2012) observed a marked increase in Evans Blue leakage in the injured cortex and in the caudate of adult rats. Moreover, many studies apply magnetic resonance imaging to noninvasively detect BBB leakage and edema after stroke injury (Knight et al., 2008; Taheri et al., 2009; Matsushita et al., 2013) after middle cerebral artery occlusion.

Finally, a strong upregulation of the GFAP was induced, indicating the activation of reactive astrogliosis during the acute phase (Li et al., 2014; Alia et al., 2021). Specifically,

the increased density of GFAP-positive cells observed in the peri-infarct cortex of MCAPT mice 1 week after photothrombosis suggests the beginning of scar formation, as previously observed in other studies (Takamatsu et al., 2002; Shen et al., 2012).

Overall, the advantages of photothrombotic occlusion of the MCA include the possibility of producing large and consistent infarcts of the cortex by occluding a large blood vessel through a nonmechanical approach, maintaining the dura mater intact, and the intracranial pressure constant. Although this model requires a craniotomy, one of the main advantages of this method includes the relatively slight invasiveness and the high degree of reproducibility (Yao et al., 2003). Considering the extended edema and the high mortality rate observed, we deem the damage induced by the photothrombotic occlusion of the distal branch of the MCA to be severe. Indeed, our model aims at reproducing a severe stroke to study the acute consequences caused by large-vessel occlusion, and the high mortality observed is attributable to the high reproducibility of the model. Conversely, in human patients, the pathophysiological insurgence of ischemia is characterized by higher variability both in terms of occlusion site and comorbidities, thus resulting in a wider spectrum of patient outcomes. However, the photothrombotic model may allow controlling of the severity of the injury by tuning the irradiation time and the dye concentration (Macrae, 2011). Moreover, our model can also be applied to induce ischemia in neonatal mice. As previously assessed by Maxwell and Dyck (2005) the photothrombotic stroke model has several advantages with respect to conventional methods to induce damage in neonatal mice, including transient and permanent MCA occlusion. Indeed, the surgical difficulties of these approaches, due to MCA exposure and filament insertion are exacerbated when working with neonatal mice. Conversely, thanks to the transparency of pup skulls (Jia et al., 2018), the distal branch of the MCA is clearly visible, thus avoiding bone thinning or craniotomy for laser irradiation.

Since half of all ischemic strokes occur in MCA territory, the development of a reproducible mouse model of stroke mimicking large thromboembolic stroke in humans is crucial in preclinical animal studies. Moreover, an animal stroke model that better resembles the pathophysiology of human ischemic stroke allows the generation of preclinical datasets suitable for investigating network dynamics and functional biomarkers of poststroke recovery (Adam et al., 2020; Mascaro et al., 2020; Cecchini et al., 2021; Kreuz et al., 2022; Scaglione et al., 2022). Finally, this approach that, to our knowledge, has never been applied in mice, will allow vascular recanalization in future experiments by illuminating the occluded vessel with a specific wavelength, as previously demonstrated in rats (Watson et al., 2002; Yao et al., 2003). The light-induced recanalization will foster the investigation of the neurovascular mechanisms underneath the ischemic progression and will allow testing of neuroprotectant agents such as glyburide (Sheth et al., 2016, 2018). Indeed, previous clinical trials have shown that glyburide reduces brain swelling after ischemia, thus improving patients' survival (Sheth et

al., 2014; Simard et al., 2014). In particular, this neuroprotective agent has been proven to be effective in large hemispheric strokes at risk of cerebral edema. Indeed, since our novel stroke model induces alteration of BBB permeability and consequent brain edema, we believe that glyburide might be an appropriate pharmacological agent to be tested. The photothrombotic occlusion of the distal MCA model was developed thanks to a bidirectional collaborative approach between preclinical and clinical researchers [i.e., the TREES (Translational Research on Stroke) Study group]. The close collaboration between clinics and research is essential to facilitate the translation of mechanistic insights offered by animal models to the bedside and to build meaningful experimental studies based on real clinical needs (Conti et al., 2021).

References

- Adam I, Cecchini G, Fanelli D, Kreuz T, Livi R, di Volo M, Allegra Mascaro AL, Conti E, Scaglione A, Silvestri L, Pavone FS (2020) Inferring network structure and local dynamics from neuronal patterns with quenched disorder. *Chaos Solitons Fractals* 140:110235.
- Alia C, Cangì D, Massa V, Salluzzo M, Vignozzi L, Caleo M, Spalletti C (2021) Cell-to-cell interactions mediating functional recovery after stroke. *Cells* 10:3050.
- Allegra Mascaro AL, Letizia A, Conti E, Lai S, Di Giovanna AP, Spalletti C, Alia C, Panarese A, Scaglione A, Sacconi L, Micera S, Caleo M, Pavone FS (2019) Combined rehabilitation promotes the recovery of structural and functional features of healthy neuronal networks after stroke. *Cell Rep* 28:3474–3485.e6.
- Balbi M, Vanni MP, Silasi G, Sekino Y, Bolanos L, LeDue JM, Murphy TH (2017) Targeted ischemic stroke induction and mesoscopic imaging assessment of blood flow and ischemic depolarization in awake mice. *Neurophotonics* 4:e035001.
- Balkaya M, Kröber JM, Rex A, Endres M (2013) Assessing post-stroke behavior in mouse models of focal ischemia. *J Cereb Blood Flow Metab* 33:330–338.
- Belayev L, Busto R, Zhao W, Ginsberg MD (1996) Quantitative evaluation of blood-brain barrier permeability following middle cerebral artery occlusion in rats. *Brain Res* 739:88–96.
- Braeuning S, Kleinschnitz C (2009) Rodent models of focal cerebral ischemia: procedural pitfalls and translational problems. *Exp Transl Stroke Med* 1:8.
- Candelario-Jalil E, Dijkhuizen RM, Magnus T (2022) Neuroinflammation, stroke, blood-brain barrier dysfunction, and imaging modalities. *Stroke* 53:1473–1486.
- Carmichael ST (2005) Rodent models of focal stroke: size, mechanism, and purpose. *NeuroRx* 2:396–409.
- Cecchini G, Scaglione A, Allegra Mascaro AL, Checcucci C, Conti E, Adam I, Fanelli D, Livi R, Saverio Pavone F, Kreuz T (2021) Cortical propagation tracks functional recovery after stroke. *PLoS Comput Biol* 17:e1008963.
- Clark TA, Sullender C, Kazmi SM, Speetles BL, Williamson MR, Palmberg DM, Dunn AK, Jones TA (2019) Artery targeted photothrombosis widens the vascular penumbra, instigates peri-infarct neovascularization and models forelimb impairments. *Sci Rep* 9:2323.
- Conti E, Piccardi B, Sodero A, Tudisco L, Lombardo I, Fainardi E, Nencini P, Sarti C, Allegra Mascaro AL, Baldereschi M (2021) Translational stroke research review: using the mouse to model human futile recanalization and reperfusion injury in ischemic brain tissue. *Cells* 10:3308.
- Conti E, Scaglione A, de Vito G, Calugi F, Pasquini M, Pizzorusso T, Micera S, Allegra Mascaro AL, Pavone FS (2022) Combining optogenetic stimulation and motor training improves functional

- recovery and perilesional cortical activity. *Neurorehabil Neural Repair* 36:107–118.
- Dietrich WD, Watson BD, Busto R, Ginsberg MD, Bethea JR (1987) Photochemically induced cerebral infarction. I. Early microvascular alterations. *Acta Neuropathol* 72:315–325.
- Fernandez-Lopez D, Faustino J, Daneman R, Zhou L, Lee SY, Derugin N, Wendland MF, Vexler ZS (2012) Blood–brain barrier permeability is increased after acute adult stroke but not neonatal stroke in the rat. *J Neurosci* 32:9588–9600.
- Gonzalez CLR, Kolb B (2003) A comparison of different models of stroke on behaviour and brain morphology. *Eur J Neurosci* 18:1950–1962.
- Guyenet SJ, Furrer SA, Damian VM, Baughan TD, La Spada AR, Garden GA (2010) A simple composite phenotype scoring system for evaluating mouse models of cerebellar ataxia. *J Vis Exp* (39): e1787.
- Howells DW, Porritt MJ, Rewell SSJ, O’Collins V, Sena ES, van der Worp HB, Traystman RJ, Macleod MR (2010) Different strokes for different folks: the rich diversity of animal models of focal cerebral ischemia. *J Cereb Blood Flow Metab* 30:1412–1431.
- Ishrat T, Sayeed I, Atif F, Stein DG (2009) Effects of progesterone administration on infarct volume and functional deficits following permanent focal cerebral ischemia in rats. *Brain Res* 1257:94–101.
- Jia J-M, Peng C, Wang Y, Zheng J, Ge W-P (2018) Control of occlusion of middle cerebral artery in perinatal and neonatal mice with magnetic force. *Mol Brain* 11:47.
- Kanemitsu H, Nakagomi T, Tamura A, Tsuchiya T, Kono G, Sano K (2002) Differences in the extent of primary ischemic damage between middle cerebral artery coagulation and intraluminal occlusion models. *J Cereb Blood Flow Metab* 22:1196–1204.
- Kenne E, Erlandsson A, Lindbom L, Hillered L, Clausen F (2012) Neutrophil depletion reduces edema formation and tissue loss following traumatic brain injury in mice. *J Neuroinflammation* 9:17.
- Knight RA, Han Y, Nagaraja TN, Whitton P, Ding J, Chopp M, Seyfried DM (2008) Temporal MRI assessment of intracerebral hemorrhage in rats. *Stroke* 39:2596–2602.
- Kreuz T, Senocrate F, Cecchini G, Checucci C, Mascaro ALA, Conti E, Scaglione A, Pavone FS (2022) Latency correction in sparse neuronal spike trains. *J Neurosci Methods* 381:109703.
- Labat-gest V, Tomasi S (2013) Photothrombotic ischemia: a minimally invasive and reproducible photochemical cortical lesion model for mouse stroke studies. *J Vis Exp* (76):50370.
- Li H, Zhang N, Lin H-Y, Yu Y, Cai Q-Y, Ma L, Ding S (2014) Histological, cellular and behavioral assessments of stroke outcomes after photothrombosis-induced ischemia in adult mice. *BMC Neurosci* 15:58.
- Macrae IM (2011) Preclinical stroke research—advantages and disadvantages of the most common rodent models of focal ischaemia. *Br J Pharmacol* 164:1062–1078.
- Mascaro ALA, et al. (2020) Experimental and computational study on motor control and recovery after stroke: toward a constructive loop between experimental and virtual embodied neuroscience. *Front Syst Neurosci* 14:31.
- Matsuno H, Uematsu T, Umemura K, Takiguchi Y, Asai Y, Muranaka Y, Nakashima M (1993) A simple and reproducible cerebral thrombosis model in rats induced by a photochemical reaction and the effect of a plasminogen-plasminogen activator chimera in this model. *J Pharmacol Toxicol Methods* 29:165–173.
- Matsushita H, Hijioka M, Hisatsune A, Isohama Y, Iwamoto S, Terasawa H, Katsuki H (2013) MRI-based analysis of intracerebral hemorrhage in mice reveals relationship between hematoma expansion and the severity of symptoms. *PLoS One* 8:e67691.
- Maxwell KA, Dyck RH (2005) Induction of reproducible focal ischemic lesions in neonatal mice by photothrombosis. *Dev Neurosci* 27:121–126.
- Menzies SA, Hoff JT, Betz AL (1992) Middle cerebral artery occlusion in rats: a neurological and pathological evaluation of a reproducible model. *Neurosurgery* 31:100–106.
- Miedel CJ, Patton JM, Miedel AN, Miedel ES, Levenson JM (2017) Assessment of spontaneous alternation, novel object recognition and limb clasping in transgenic mouse models of amyloid- β and tau neuropathology. *J Vis Exp* (123):55523.
- Mies G, Ishimaru S, Xie Y, Seo K, Hossmann KA (1991) Ischemic thresholds of cerebral protein synthesis and energy state following middle cerebral artery occlusion in rat. *J Cereb Blood Flow Metab* 11:753–761.
- Mora-Lee S, Salomé Sirerol-Piquer M, Gutiérrez-Pérez M, López T, Casado-Nieto M, Jauquicoam C, Abizanda G, Romaguera-Ros M, Gomez-Pinedo U, Prósper F, García-Verdugo J-M (2011) Histological and ultrastructural comparison of cauterization and thrombosis stroke models in immune-deficient mice. *J Inflamm (Lond)* 8:28.
- Reglodi D, Somogyvari-Vigh A, Maderdrut JL, Vigh S, Arimura A (2000) Postischemic spontaneous hyperthermia and its effects in middle cerebral artery occlusion in the rat. *Exp Neurol* 163:399–407.
- Rosenberg GA, Estrada EY, Dencoff JE (1998) Matrix metalloproteinases and TIMPs are associated with blood–brain barrier opening after reperfusion in rat brain. *Stroke* 29:2189–2195.
- Saniabadi AR, Umemura K, Matsumoto N, Sakuma S, Nakashima M (1995) Vessel wall injury and arterial thrombosis induced by a photochemical reaction. *Thromb Haemost* 73:868–872.
- Saunders NR, Dziegielewska KM, Møllgård K, and MD Habgood (2015) Markers for blood–brain barrier integrity: how appropriate is Evans blue in the twenty-first century and what are the alternatives? *Front Neurosci* 9:385.
- Scaglione A, Conti E, Allegra Mascaro AL, Pavone FS (2022) Tracking the effect of therapy with single-trial based classification after stroke. *Front Syst Neurosci* 16:840922.
- Shen J, Ishii Y, Xu G, Dang TC, Hamashima T, Matsushima T, Yamamoto S, Hattori Y, Takatsuru Y, Nabekura J, Sasahara M (2012) PDGFR- β as a positive regulator of tissue repair in a mouse model of focal cerebral ischemia. *J Cereb Blood Flow Metab* 32:353–367.
- Sheth KN, Kimberly WT, Elm JJ, Kent TA, Mandava P, Yoo AJ, Thomalla G, Campbell B, Donnan GA, Davis SM, Albers GW, Jacobson S, Simard JM, Stern BJ (2014) Pilot study of intravenous glyburide in patients with a large ischemic stroke. *Stroke* 45:281–283.
- Sheth KN, Elm JJ, Molyneaux BJ, Hinson H, Beslow LA, Sze GK, Ostwaldt A-C, del Zoppo GJ, Simard JM, Jacobson S, Kimberly WT (2016) Safety and efficacy of intravenous glyburide on brain swelling after large hemispheric infarction (GAMES-RP): a randomized, double-blind, placebo-controlled phase 2 trial. *Lancet Neurol* 15:1160–1169.
- Sheth KN, Petersen NH, Cheung K, Elm JJ, Hinson HE, Molyneaux BJ, Beslow LA, Sze GK, Simard JM, Kimberly WT (2018) Long-term outcomes in patients aged ≤ 70 years with intravenous glyburide from the phase II GAMES-RP Study of Large Hemispheric Infarction. *Stroke* 49:1457–1463.
- Shih AY, Nishimura N, Nguyen J, Friedman B, Lyden PD, Schaffer CB, Kleinfeld D (2013) Optically induced occlusion of single blood vessels in rodent neocortex. *Cold Spring Harb Protoc* 2013:1153–1160.
- Simard JM, Sheth KN, Kimberly WT, Stern BJ, del Zoppo GJ, Jacobson S, Gerzanich V (2014) Glibenclamide in cerebral ischemia and stroke. *Neurocrit Care* 20:319–333.
- Stoll G, Kleinschnitz C, Meuth SG, Braeuninger S, Ip CW, Wessig C, Nölte I, Bendszus M (2009) Transient widespread blood–brain barrier alterations after cerebral photothrombosis as revealed by gadofluorine M-enhanced magnetic resonance imaging. *J Cereb Blood Flow Metab* 29:331–341.
- Sugimori H, Yao H, Ooboshi H, Ibayashi S, Iida M (2004) Krypton laser-induced photothrombotic distal middle cerebral artery occlusion without craniectomy in mice. *Brain Res Brain Res Protoc* 13:189–196.
- Sunil S, Erdener SE, Lee BS, Postnov D, Tang J, Kura S, Cheng X, Chen IA, Boas DA, Kılıç K (2020) Awake chronic mouse model of targeted pial vessel occlusion via photothrombosis. *Neurophotonics* 7:e015005.

- Taheri S, Candelario-Jalil E, Estrada EY, Rosenberg GA (2009) Spatiotemporal correlations between blood-brain barrier permeability and apparent diffusion coefficient in a rat model of ischemic stroke. *PLoS One* 4:e6597.
- Takamatsu H, Tatsumi M, Nitta S, Ichise R, Muramatsu K, Iida M, Nishimura S, Umemura K (2002) Time courses of progress to the chronic stage of middle cerebral artery occlusion models in rats. *Exp Brain Res* 146:95–102.
- Wafa HA, Wolfe CDA, Emmett E, Roth GA, Johnson CO, Wang Y (2020) Burden of stroke in Europe: thirty-year projections of incidence, prevalence, deaths, and disability-adjusted life years. *Stroke* 51:2418–2427.
- Watson BD, Dietrich WD, Prado R, Ginsberg MD (1987) Argon laser-induced arterial photothrombosis. Characterization and possible application to therapy of arteriovenous malformations. *J Neurosurg* 66:748–754.
- Watson BD, Prado R, Veloso A, Brunschwig J-P, Dietrich WD (2002) Cerebral blood flow restoration and reperfusion injury after ultraviolet laser-facilitated middle cerebral artery recanalization in rat thrombotic stroke. *Stroke* 33:428–434.
- Yang J, Li Q, Wang Z, Qi C, Han X, Lan X, Wan J, Wang W, Zhao X, Hou Z, Gao C, Carhuapoma JR, Mori S, Zhang J, Wang J (2017) Multimodality MRI assessment of grey and white matter injury and blood-brain barrier disruption after intracerebral haemorrhage in mice. *Sci Rep* 7:40358.
- Yao H, Sugimori H, Fukuda K, Takada J, Ooboshi H, Kitazono T, Ibayashi S, Iida M (2003) Photothrombotic middle cerebral artery occlusion and reperfusion laser system in spontaneously hypertensive rats. *Stroke* 34:2716–2721.
- Zhao B-Q, Suzuki Y, Kondo K, Kawano K-I, Ikeda Y, Umemura K (2002) A novel MCA occlusion model of photothrombotic ischemia with cyclic flow reductions: development of cerebral hemorrhage induced by heparin. *Brain Res Brain Res Protoc* 9:85–92.
- Zhao Q, Memezawa H, Smith M-L, Siejö BK (1994) Hyperthermia complicates middle cerebral artery occlusion induced by an intraluminal filament. *Brain Res* 649:253–259.